

A Novel Technique for the Restoration of AFM Images Enabling an Estimated Impulse Response for the AFM to be Calculated Using Square Pillar and Cylindrical Pillar Samples

Ahmed M. Ahtaiba, Munther A. Gdeisat, David R. Burton and Francis A. Lilley

Abstract—All atomic force microscope (AFM) images suffer from distortions, which are principally produced by the interaction between the measured sample and the AFM tip. The atomic force microscope (AFM) is a very important instrument for use in nanotechnology and biology since it can be used to measure a wide variety of objects, such as nano-particles and cells, either in air or liquid. However, the images that are measured using AFM are distorted because of both the influence of the tip geometry and the dynamic response of the instrument. This influence means that the images do not accurately represent the real shape of the measured particles or cells. Therefore, it is necessary to reconstruct the AFM tip shape. This paper proposes a new approach (impulse response technique) to reconstruct the AFM tip shape from either a square or cylindrical pillar sample that is measured using AFM. Once the tip shape is known, a deconvolution process is carried out between the estimated tip shape and typical AFM ‘distorted’ images in order to reduce the distortion effects. The experimental results and the computer simulations validate the performance of the proposed approach, in which it is shown that the AFM image accuracy has been significantly improved. The suitability of this novel approach for restoring AFM images has been confirmed using both computer simulation and also with real experimental AFM images. The blind tip estimation approach is an industrial and research standard algorithm for the restoration of AFM images. We therefore also compare the proposed algorithms with the blind tip estimation algorithm, via the use of both computer simulations and real AFM images, and our algorithm is shown to give enhanced results when compared with the blind tip estimation approach.

Index Terms—Atomic force microscope, AFM, image restoration, deconvolution, and image morphology.

I. INTRODUCTION

THE atomic force microscope (AFM) is a very useful tool in the biomedical engineering [1] and microelectronics [2] industrial sectors. An AFM image is a distorted representation of the sample, due to the convolution effect which is produced by the finite size of the AFM tip and the dynamic response of the instrument. The image restoration problem has been studied by many researchers in terms of firstly determining the cantilever tip shape for the AFM and subsequently using it to restore the AFM images. AFM images were restored by Pingali et al [3] using mathematical morphological operators. The AFM tip shape was reconstructed from AFM images of known samples by Keller et al. [4], who used the reconstructed AFM tip for the restoration of the AFM images. Blind tip reconstruction was an approach that was developed by Villarrubia et al. [5], which is based on mathematical morphology methods. Dongmo [6] used this algorithm for reconstructing a stylus profilometer tip and then a comparison was carried out between the reconstructed tip shape and its SEM image. Subsequently Todd [7] showed that noise in the AFM image causes a distortion in the tip estimation and proposed an approach to improve the algorithm. Recently Tranchida [8] has taken the effects of operating parameters (for instance, sampling intervals and instrumental noise) into consideration in the practical use of the algorithm. He subsequently introduced some guidelines for the use of the blind estimation algorithm and the appropriate experimental conditions that are relevant to the algorithm.

This static formulation of the image restoration problem ignores other dynamic parameters that affect the image acquisition process for the AFM, such as the scanning speed, the response of the x, y and z piezo materials, and the bandwidth of the feedback loop system. As is well-known in digital image processing theory, the impulse response of a linear time invariant system “fully characterises” this system. This implies that our proposed algorithm’s aim of finding an estimate of the impulse response of the AFM should inherently take all these parameters into consideration and should produce a better and more faithful image restoration algorithm than those that already exist in the literature.

The first essential step at the front-end of digital image processing systems is that of capturing digital images. Many distortions occur during the image acquisition process and these distortions should be eliminated, or alleviated, by using image restoration algorithms. Examples of systems where

Manuscript received August 20, 2011; revised May 18, 2012.

The authors are with The General Engineering Research Institute (GERI), Liverpool John Moores University, James Parsons Building, Byrom Street, Liverpool L3 3AF, UK. Corresponding author’s email is A.M.Ahtaiba@2009.ljmu.ac.uk, m.a.gdeisat@ljmu.ac.uk.

these distortions occur are in astronomical imaging using telescopes, inconfocal microscopy, computedtomographic (CT) scanners and many other applications. These are similar research problems to that of the image restoration of AFM images [9]-[11].

In this paper we propose two variants of a new method (referred to here as the impulse response technique), which are suitable for estimating the AFM tip shape from a typical AFM image produced by measuring either a square or cylindrical pillar sample. Both computer simulation and experimental results were used for estimating the AFM tip shape. In both the computer simulations and the experimental results, a Lucy-Richardson deconvolution process was used between the estimated AFM tip shape and the raw AFM image in order to obtain a more accurate restored AFM image [12]. Also we determine the three-dimensional AFM tip shape (impulse response of AFM) using experimental results that are gathered from measuring the cylindrical sample via AFM. Once the AFM tip is reconstructed, the Lucy- Richardson algorithm [13] is used to calculate the deconvolution between the resultant AFM tip and the blurred raw AFM image. This produces a more accurate AFM image. Finally, we compare the results of our proposed algorithms with the blind tip estimation algorithm and the proposed algorithms are shown to provide superior performance.

II. THE IMPULSE RESPONSE ALGORITHM USING A SQUARE PILLAR SAMPLE

It is proposed here that the determination of the three-dimensional impulse response of the AFM could be performed by taking the following steps. A standard AFM calibration sample that contains a grid of square pillars, with dimensions that are accurately known *a priori* to their measurement [20] is first measured using contact mode AFM for a region of interest that encompasses an entire single raised square pillar. The traceable height of the square pillar is nominally 100 nanometres. The raw 3D topographical image that is produced by the AFM for the sample contains the square pillar's surface profile, however this profile is broadened due to the convolution process between the cantilever tip and the square pillar sample. Digital image processing algorithms are then used to determine the exact location of the square pillar within the image. As its height is known *a priori*, those pixels that belong to the top surface of the square pillar are subsequently subtracted and are thus removed from the image, as follows. Firstly, the four sections that represent the impulse response of the AFM were numbered, as shown in Fig. 1(a). Then, sections 1 and 2 were translated towards each other. Next, sections 3 and 4 were also moved towards each other. Finally, we moved both sections 1, 2 and also sections 3, 4 simultaneously towards the centre of the square, as shown in Fig. 1(b). The resultant image can now be considered to be a representation of the three-dimensional impulse response of the AFM.

III. AFM TIP ESTIMATION USING A SQUARE PILLAR SAMPLE

This paper presents a new technique for estimating the AFM tip shape from the square pillar sample using a new impulse response method. The proposed approach uses a tip characterizer (square pillar sample) [14-16]. The raw AFM image of the square pillar sample is considered to be produced as a result of a convolution between the shape of the sample and the AFM tip. Thus, the AFM tip can be reconstructed by eliminating the effects of the tip characterizer topography from the AFM image of the square sample, at the same time taking into account dynamic effects of the instrument. We have used a tip characterizer that consists of a standard square pillar sample and the impulse response approach for eliminating the effects of the tip characterizer geometry and dynamics from the AFM image. In this paper we will show that the proposed approach of using an impulse response method is effective for estimating 3-D tip geometry, which then can be used in the restoration of more accurate AFM images.

A. Computer Simulation

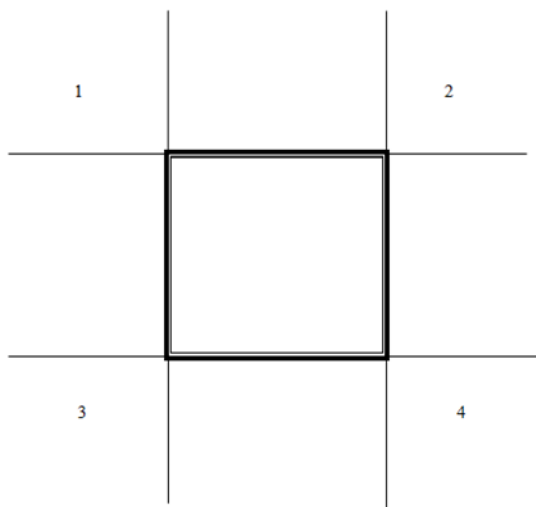
In the computer simulation, we have constructed computer models for both the AFM tip and the sample, in which the tip has a pyramidal shape and the sample has the shape of a raised square pillar, as depicted in Figs. 2(a) and 2(b) respectively. An AFM image of the square pillar sample would be represented by a convolution process between the sample topography and the pyramidal tip. It is clear from Fig. 2(c) that after applying a convolution process between the simulated sample and simulated tip, the AFM image is now distorted by the AFM tip shape and no longer accurately represents the true sample topography. This type of distortion is representative of the results that are produced by any typical AFM instrument. In order to improve the AFM image, it is therefore necessary to obtain information about the AFM tip shape. Once the tip shape is known, the reverse process of the convolution procedure (which is a deconvolution) can be applied between the distorted AFM image and the reconstructed tip shape in order to remove this distortion found within the raw AFM image, as produced by the instrument. The image of the simulated square pillar sample is then thresholded. The goal of this thresholding operation is to segment the grey level image into two regions, namely the background region and the square pillar object itself. The optimal threshold value can be considered to be a grey level that separates an object region and a background region, without compromising the object's integrity [17].

Next, the outer boundary of the square pillar was determined using the Canny edge detection algorithm, which is well known as being an optimal edge detector. Once the outer boundary is detected, as illustrated in Fig 2(d), the pixels that belong to the image of the square pillar are eliminated. At the same time the data associated with the effects of the AFM tip, which are present around the outer perimeter of the eliminated square, are translated towards a position at the centre of the previously removed square. The resultant image, which is illustrated in Fig. 3, is an approximation of the impulse response of the AFM.

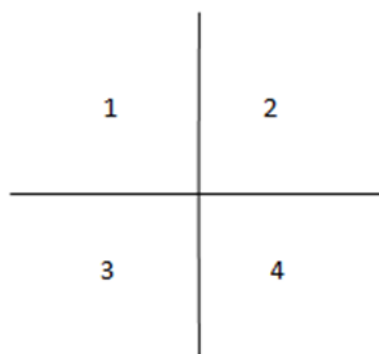
Any real experimental AFM topographic image may be regarded as being the result of the ‘true’ surface topography of the object $S(x,y)$ that has been degraded by instrumental noise $W(x,y)$. Thus the AFM image $I(x,y)$ can be represented as being a convolution of the actual topographical image $S(x,y)$ and a degrading, or impulse response function $h(x,y)$, as in the following equation. Where x, y are the indices of pixels in the image.

$$I(x,y) = S(x,y) * h(x,y) + W(x,y) \tag{1}$$

Where $I(x,y)$ is the degraded AFM image, $S(x,y)$ is the original ‘true’ sample topography, (*) indicates the 2D convolution effect between the sample and the tip, and $W(x,y)$ is a noise term.



(a)



(b)

Fig. 1. Illustrates the process of eliminating the square pillar from the image using the impulse response technique. (a) The selected four regions 1,2,3,4 that contain information about the AFM tip; (b) moving the four sections 1, 2, 3, 4 towards the middle of the central square. This results in eliminating those pixels that belong to the square pillar and the remaining result is an approximation of the impulse response of the AFM.

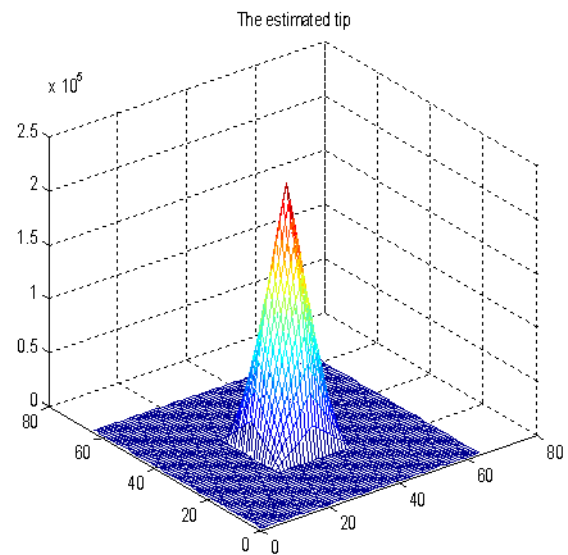


Fig. 3. Shows the simulation results showing the 3D image of the reconstructed tip shape.

Fig. 4(a) shows the two dimensional image of the square pillar sample that is analogous to a real AFM image, as it is a convolution between the pyramidal tip and the object’s surface topography. Fig. 4(b) shows the reconstructed image after applying a Lucy-Richardson deconvolution process between the reconstructed AFM tip shape and the blurred image of the square. The result of the deconvolution process, which comprises the reconstructed image, is slightly improved when compared with the original image.

B. Experimental Results for Estimating 3-D AFM Tip Shape

The three-dimensional impulse response of the AFM could be determined by performing the following steps. Measuring the topography of a standard AFM calibration sample using the AFM, as shown in Fig.5(a), that contains a raised square pillar with accurately known dimensions *a priori* to measurement. The 2-D topographical image that is produced by the AFM for the sample contains information about the square pillar’s 3D profile, but this is broadened due to the convolution effect between the 3D tip shape and the square pillar’s true topography. Digital image processing techniques, such as thresholding and Canny edge detection, were used to determine the exact location of the square pillar within the image, as is illustrated in Figs. 5(b) and 5(c), respectively. As the height of the square is known *a priori*, the pixels that represent the square pillar may be eliminated by moving the inherent image distortions, that have been introduced due to convolution effects, to the centre of the image of the square. The resultant image may be considered to represent the three-dimensional AFM tip shape using the impulse response method, and this is illustrated in Fig.5(d). Also, this image is considered to approximate the impulse response of the AFM.

IV. RESTORATION OF EXPERIMENTAL AFM IMAGES

Restoration of images that are subsequently produced by the AFM can be carried out by performing a deconvolution process between the raw AFM image that is acquired directly from the instrument and the approximated AFM impulse response that was described in the previous section. Many algorithms can be applied here to perform this task, such as the Wiener, Regularized filter, Lucy-Richardson, and Blind deconvolution algorithms [13].

The widely used Lucy-Richardson algorithm uses the *a priori* information of non-negativity and flux conservation. It produces a restored AFM image through an iterative method. The idea is to imagine that the ideal AFM image is convolved with the impulse response of the AFM. The Lucy-Richardson algorithm maximizes the likelihood function of the image, which is modeled using Poisson statistics. The Lucy-Richardson algorithm uses such an iterative algorithm, as shown in (2).

$$f_{k+1}(x, y) = f_k(x, y) \frac{I(x, y) * h(-x, -y)}{[h(x, y) * f_k(x, y)] * h(-x, -y)} \quad (2)$$

Where $h(-x, -y)$ is the transpose of the impulse response of the system, $f_k(x, y)$ is the previous estimate of the AFM image, $h(x, y)$ is the impulse response of the AFM system, and $f_{k+1}(x, y)$ is the current estimate of the AFM image.

The derivation and theory of operation of this algorithm has been described in detail in the original papers by Lucy [18] and Richardson [19].

Fig. 6(a) shows an AFM topographical image of a single selected square pillar, produced by measuring a sub-region of the real sample that contains a grid of square pillars that is presented in Fig. 7. The restored AFM image after applying a Lucy-Richardson deconvolution algorithm is depicted in Fig. 6(b). As a result it can clearly be seen that the level of distortion in the restored image has been reduced when compared with the original raw AFM image.

Figs. 7(a) and 7(b) respectively, illustrate the simulations of the blurred AFM image and also the resultant restored AFM image that was produced by applying the deconvolution process. As a result of applying the deconvolution algorithm, it can be seen from Fig. 7(b) that the quality of the restored AFM image has been improved by removing the effects of the convolution by the AFM tip shape from the original blurred image.

V. THE IMPULSE RESPONSE ALGORITHM USING A CYLINDRICAL PILLAR SAMPLE

The tip is the part of AFM that in fact touches (or comes very close to touching) the surface of the sample and it is mounted at the end of a cantilever. As with any probing instrument, the tip of the cantilever is considered to be the most essential part of the AFM instrument. Originally tips had a pyramidal shaped structure and were produced from either silicon dioxide, or silicon nitride. This paper suggests a new approach to estimate the tip shape more faithfully by using an impulse response technique. The resulting AFM topographical image, as produced by typical AFM instruments, is a function of both the shape of the sample and

that of the tip. Thus, the tip shape can be estimated by removing the effects of the sample characteriser topography from the AFM image [15], [16].

The proposed method uses a sample characteriser consisting of a standard grid of cylindrical columns along with the impulse response technique for removing the effects of the sample characteriser geometry from the AFM image [20]. The proposed method of using an impulse response technique is effective for estimating 3-D tip shape, which is then used in the restoration of more faithful AFM images via tip shape deconvolution.

The determination of the three-dimensional impulse response of the AFM can be performed by taking the following steps. A standard AFM calibration sample, shown in Fig. 8(a), that contains a grid of cylinders [20] with traceable *a priori* accurately known dimensions, is measured using the AFM, for a region of interest encompassing just a single cylinder in its entirety. The diameter and the height of the cylinder are 1000 nm and 106 nm respectively. The distance between the centres of two consecutive columns is nominally 5 μm . The 3D topographical image that is produced by the AFM for the sample contains the cylinder's 3D profile, but this is broadened due to the convolution between the cantilever tip and the cylinder. This broadening effect is illustrated in Fig. 8(b). Digital image processing algorithms have then been used to determine the exact location of the cylinder within the image, as its height is known *a priori*, and those pixels that belong to the cylinder have been subsequently subtracted and thereby removed from the image. The inherent image distortions that have been introduced due to the convolution effect will remain in the image after this subtraction, as is depicted in Fig. 8(c). The resultant image contains an empty circular region, i.e., zero-valued pixels that have replaced the pixels that belong to the cylinder. Finally the image is processed by moving the data which were located around the periphery of the eliminated cylinder inwards towards the centre of the cylinder [22]. The resultant image which is shown in Fig. 8(d) can be considered to be the three-dimensional impulse response of the AFM.

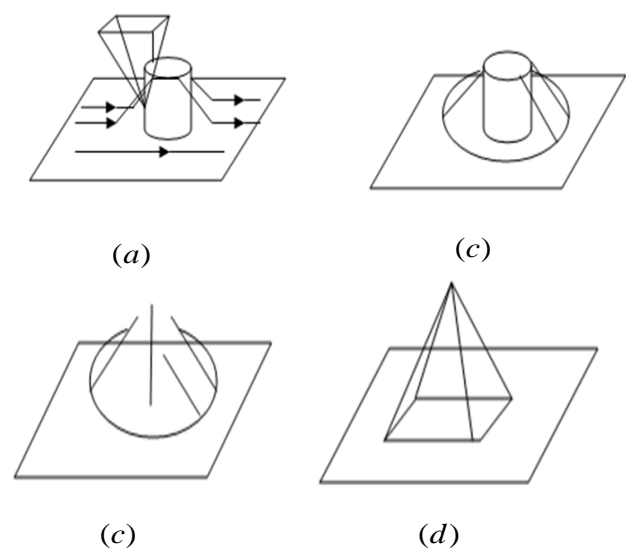


Fig. 8 Illustrates the proposed procedure for estimating the AFM impulse response: (a) measuring a standard sample that contains a cylinder with known dimensions using the AFM, (b) determining the location of both the

cylinder and the edge distortion effects region within the image; (c) removing the pixels that belong to the cylinder from the image; (d) extracting the impulse response of the AFM.

VI. AFM TIP ESTIMATION USING A CYLINDRICAL PILLAR SAMPLE

A. Computer Simulation

Figs. 9(a) and 9(b) illustrate a three-dimensional computer simulation of the sample and the tip, respectively. Computer models of the cylindrical sample and the pyramidal tip were first constructed. The simulated image representing the raw AFM measured topographic image of the cylindrical sample was calculated from the sample and the tip by dilation. As a result the dilation of the sample by a tip can introduce significant inaccuracy in an AFM image when the tip scans the sample as is shown in Fig. 9(c). The outer boundary of the image of the cylinder has been determined by using the Canny edge detection algorithm [12]. Next, the outer boundary was expanded to allow inclusion of the tip broadening distortion data, which are available around the dilated cylinder. Then, Bresenham's line algorithm was applied for removing the cylinder and moving the tip data radially inwards towards the centre of the removed cylinder's original location. The result is the estimated AFM tip shape using this impulse response technique, and this is illustrated in Fig. 9(d).

When the shape tip is estimated, the restored AFM image can be obtained by applying an erosion process between the dilated image and the reconstructed tip shape.

Figs. 10(a) and 10(b) depict the original image dilated by the AFM tip and the restored AFM image after applying the erosion operation, respectively. As a result, it is evident that the restored image is a better representation of the true image topography than the dilated image. In other words, the distortion due to the dilation operation between the pyramidal tip and the cylindrical sample is reduced when compared to the blurred image when the erosion operation is carried out between the estimated tip and the blurred image.

B. Experimental Results

We used contact mode AFM to measure a standard sample with precisely known dimensions, that is constructed from silicon and which consists of a 2D array of small cylindrical columns. After this AFM measurement a single column was selected from the image and the same steps for image processing that were explained in the previous computer simulation example were implemented here on this sub-image. A threshold was chosen for determining the area of the top of the column within the AFM image, which is approximately an entire circle as is shown in Fig. 11(a). The outer boundary and the centre of the column were determined using the Canny edge detection algorithm and the result of this edge detection is depicted in Fig. 11(b). Then we expanded the outer boundary and its size was arbitrarily chosen in order to estimate the associated tip distortion data that were available around the periphery of the column, as illustrated in Fig. 11(c). Next, we applied Bresenham's line algorithm to move the tip data that were located around the outer boundary of the cylinder radially inwards towards the centre of the previously removed cylinder and Fig. 11(d)

shows the result, which is the 3-D estimated AFM tip shape using the impulse response technique.

VII. RESTORATION OF EXPERIMENTAL AFM IMAGES

Restoration of subsequent images that are produced by the AFM when using the same tip and scan rate can be carried out by performing a deconvolution process between the raw AFM image that is acquired by the instrument and the impulse response that was found as detailed in the previous section. Many algorithms can be used such as the Wiener, regularized filter, Lucy-Richardson, and blind deconvolution algorithms [12]. Figs. 12(a) and 12(b) compare the AFM image of an array of columns and the restored AFM image after applying the Lucy-Richardson deconvolution method. This comparison indicates that the Lucy-Richardson deconvolution approach works properly and the restored image is again clearly improved as is depicted in Fig. 12(b).

IX. BLIND TIP ESTIMATION ALGORITHM

Blind tip estimation algorithms are a standard method that are used for the restoration of AFM images and rely on set theory and morphological operations [5], [21]. Here we introduce Villarrubia's method, which is based upon set theory, which we shall use as a benchmark for comparison of the novel method that was proposed in the previous sections. Using this technique, where the surface topography is unknown, it is possible to estimate the tip shape from the original AFM image of the sample. The image of the object is obtained by the dilation of the sample and the reflection of the tip P .

$$I = S \oplus P \quad (3)$$

Where I is the image of the sample, S is the genuine surface topography, and $(P = -T)$ is the reflection of the tip T . In the case where the actual surface topography is known, then using erosion, the estimated tip topography is;

$$P_r = I \ominus S \quad (4)$$

Where P_r is the estimated 3D surface of the tip. Sample reconstruction by erosion can be written as;

$$S_r = I \ominus P \quad (5)$$

Where S_r is the reconstructed sample. The iterative process for blind tip estimation is defined by the following equation:

$$P_{i+1} = \bigcap_{\vec{x} \in I} [(I - \vec{x}) \oplus P'_i(x)] \cap P_i \quad (6)$$

In Equation (6), the calculation of the $(i + 1)$ th iteration result is based on the (i) th result. Where \vec{x} is a point of interest in the image I .

$$P'_i(X) = (\vec{x} - I) \cap P_i \quad (7)$$

$P'_i(X)$ is a set of points in P_i that can contact the image I at a point of interest \vec{x} , with the apex point contained in the image I .

At convergence, the result of the estimated tip shape P_r can be determined as being:

$$P_r = \lim_{i \rightarrow \infty} P_i \quad (8)$$

Upon convergence, the final result gives the best estimate of the tip shape that has been obtained by the blind reconstruction approach.

A. Experimental Results

A real sample that contains square columns was measured using an AFM in contact mode. Fig.(13) shows the experimental results for the blind tip reconstruction process, where Figure. 13(a) illustrates the 3D estimated tip image that has been reconstructed using the blind tip estimation approach. The original image of the real sample that was measured by the AFM instrument is shown as a raw AFM image in Fig. 13(b). This image has been created due to a dilation of the sample topology by the AFM tip shape which was used to measure the sample. Finally an erosion operation upon the original (dilated) image by the estimated tip shape has been used for reconstructing the image of the sample which is shown in Fig.13(c). As a result, the restored image can be seen to be only slightly improved, when compared with the original image.

VIII. CONCLUSION

The impulse response algorithms using the square pillar sample and the cylinder pillar sample have been demonstrated to be a useful tool in restoring AFM images. Both the computer simulations and the experimental results for the impulse response techniques using the square and cylindrical pillar samples have produced results that show improvements in the quality of the restored AFM images after the application of the Lucy-Richardson deconvolution algorithm. Finally we have compared our proposed algorithms with an existing standard approach to AFM image restoration that uses blind tip estimation and the results shown here indicate that application of the proposed algorithms leads to measurement results that are superior in quality to those that are produced by blind tip estimation.

REFERENCES

- [1] K. Angelika, K. Christine, L. Alois, and B. Mizaikoff, "AFM - tip-integrated amperometric microbiosensors: high-resolution imaging of membrane transport", *Angewandte Chemie International Edition*, vol. 44, pp. 3419-3422, 2005.
- [2] J. Schneir, M. C. Sweeney, and T. H. Mcquaid, "In fourth workshop on industrial applications of scanning probe microscopy, NIST Gaithersburg, MD, USA, pp 30-31, 1997.
- [3] G. S. Pingali and R. Jain, "Restoration of Scanning Probe Microscope Images," In *Application Of Computer Vision*, Palm Springs, CA, USA, 1992.
- [4] D. J. Keller and F. S. Franke, "Envelope Reconstruction of Probe Microscope Images," *Surface Science*, P. 11, 1993.
- [5] J.S. Villarrubia, "Algorithms for Scanned Probe Microscope Image Simulation Surface Reconstruction and Tip Estimation," *Journal of Research of The National Institute of Standards and Technology*, Vol. 04, PP. 425-454, 1997.
- [6] L.S. Dongmo, J.S. Villarrubia, S.N. Jones, T.B. Renegar, M.T. Postek, and J.F. Song, "Experimental Test of Blind Tip Reconstruction for Scanning Probe Microscopy," *Ultramicroscopy*, Vol. 85, PP. 141 - 153, 2000.
- [7] T. Brain and E. Steven, "A Method to Improve the Quantitative Analysis of SPM Images at the Nanoscale" *Surf. Sci.*, 2001.
- [8] D. Tranchida, S. Piccarolo, and R.A.C. Deblieck, "Some Experimental Issues of AFM Tip Blind Estimation: The Effect of Noise and Resolution," *Meas. Sci. Technol.*, Vol. 17, PP. 2630 - 2636, 2006.
- [9] M. Bertero and P. Boccacci, "Image restoration methods for the large binocular telescope", *Astronomy & Astrophysics Supplement Series*, vol. 147, No.2, pp. 323-333, 2000.
- [10] P. J. Verveer, M. J. Gemkow and T. M. Jovin, "A comparison of image restoration approaches applied to three-dimensional confocal and wide-field fluorescence microscopy", *Journal of Microscopy*, vol. 193, No. 1, pp. 50-61, 1999.
- [11] N. Nakamori, K. Tsukamoto and T. Tsunoo, "Image restoration of cone-beam CT images using wavelet transform", *Proceedings of The SPIE- The International Society for Optical Engineering*, vol. 3338, No.2, pp. 1275-1282, 1998.
- [12] R. Gonzalez, *Digital Image Processing*, Second Edition, Gatesmark publishing, 2008.
- [13] R. Gonzalez, "Digital Image Processing Using Matlab", Second Edition, Gatemark Publishing, 2009.
- [14] H. Yasuhiko, S. Havato, H. Sumio, "Estimation of three dimensional Atomic Force Microscope tip shape from Atomic Force Microscope image for accurate measurement", *Japanese Journal of Applied physics.*, vol. 47, No. 7, pp. 6186-6189, 2008.
- [15] N. Masao, N. Hideo, K. Kenji and M. Takahiro, "Critical dimension measurement in nanometer scale by using Scanning Probe Microscopy", *Japanese Journal of Applied physics*, vol. 35, pp. 4166-4177, 1996.
- [16] N. Masao, N. Hideo, K. Kenji, I. Kazumi and M. Katsumi, "Metrology of Atomic Force Microscopy for Si nano-structures", *Japanese Journal of Applied physics*, vol. 34, pp. 3382-3387, 1995.
- [17] T. Wenbing, J. Hai, Z. Yimin, L. Liman, and W. Desheng, *IEEE Transactions on systems*, vol. 38, No. 5, pp. 96-99, 2008.
- [18] L. B. Lucy, "An iterative technique for the rectification of observed distributions", *The Astronomical Journal*, vol. 79, No.6, pp. 745-754, 1974.
- [19] W. H. Richardson, "Bayesian-based iterative method of image restoration", *Journal of the optical society of America*, vol. 62, No.1, pp. 55-59, 1970.
- [20] Budget Sensors Company for fabrication of AFM calibration samples. <http://www.budgetsensors.com/HS-100MG.html>.
- [21] T. Fenglei, Q. Xiaoping, and J. S. Villarrubia, "Blind estimation of general tip shape in AFM imaging", *Ultramicroscopy*, vol. 109, pp. 44-53, 2008.
- [22] A. Ahtaiba, M. Gdeisat, D. Burton, F. Lilley, and M. Murphy, "A Novel Approach to the Restoration of AFM Images Employing an Estimated Impulse Response for the AFM Calculated Using a Square Pillar Sample", *World Congress on Engineering*, vol.2, Jul. 2011, pp. 1657-1662.

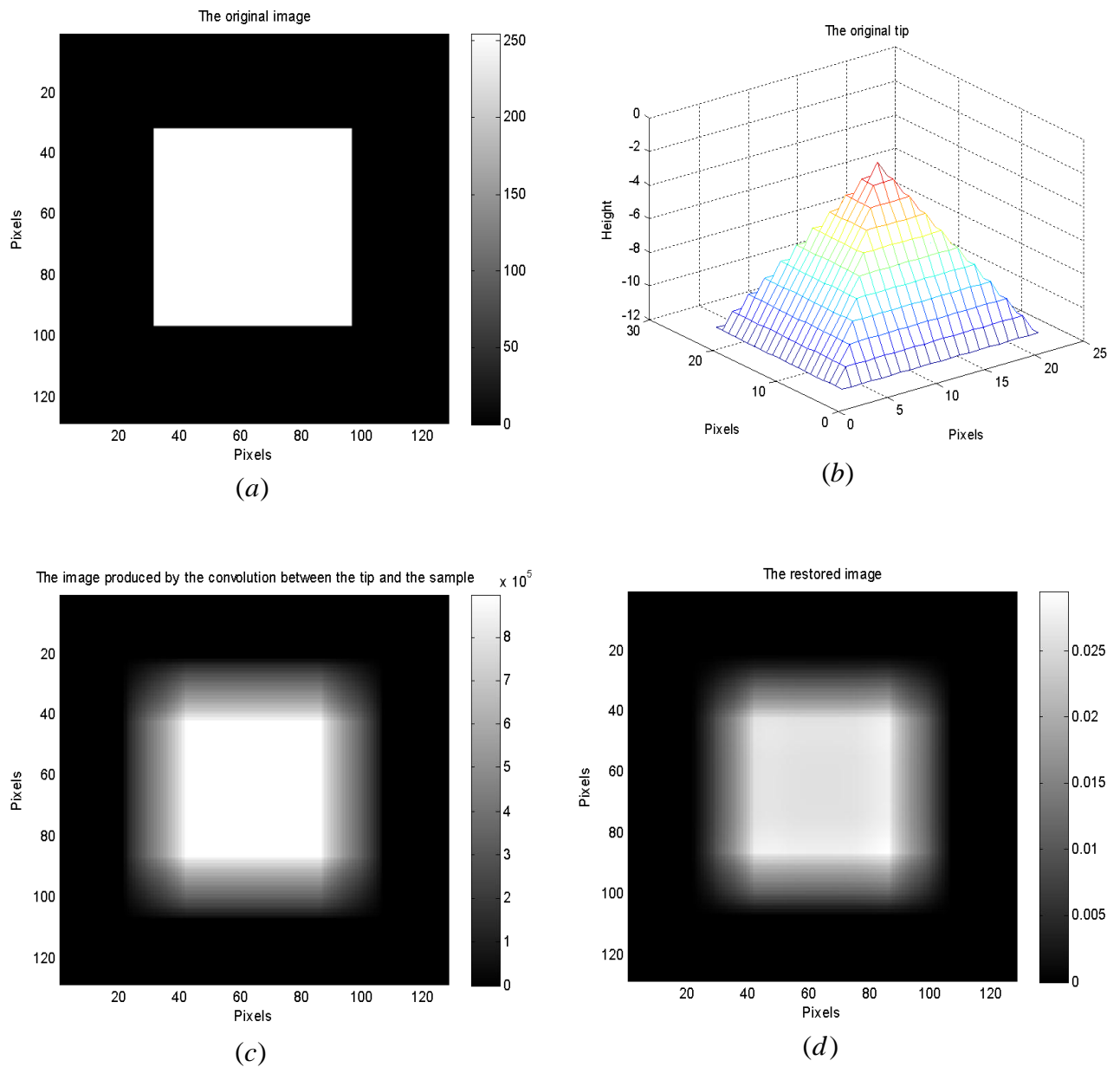


Fig. 2. Depicts the simulation results for the impulse response technique using a square pillar sample. (a) the square pillar sample; (b) the AFM tip; (c) the image of the square sample that is produced by the convolution effect between the square pillar sample and the original AFM tip; (d) The reconstructed image.

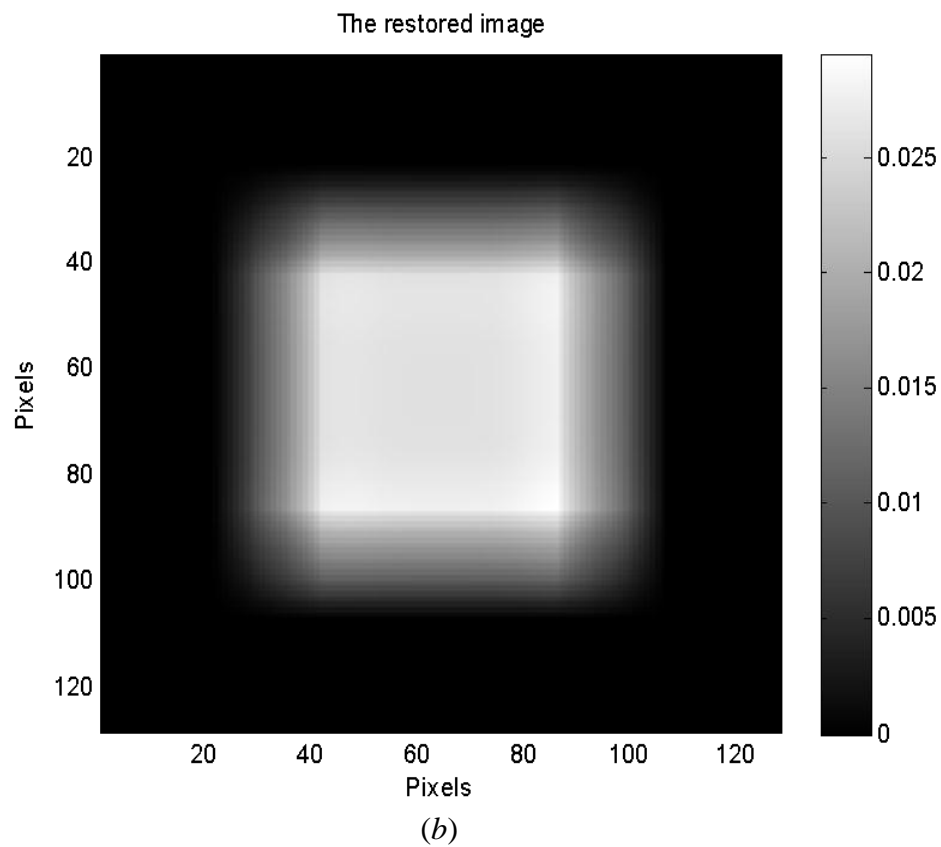
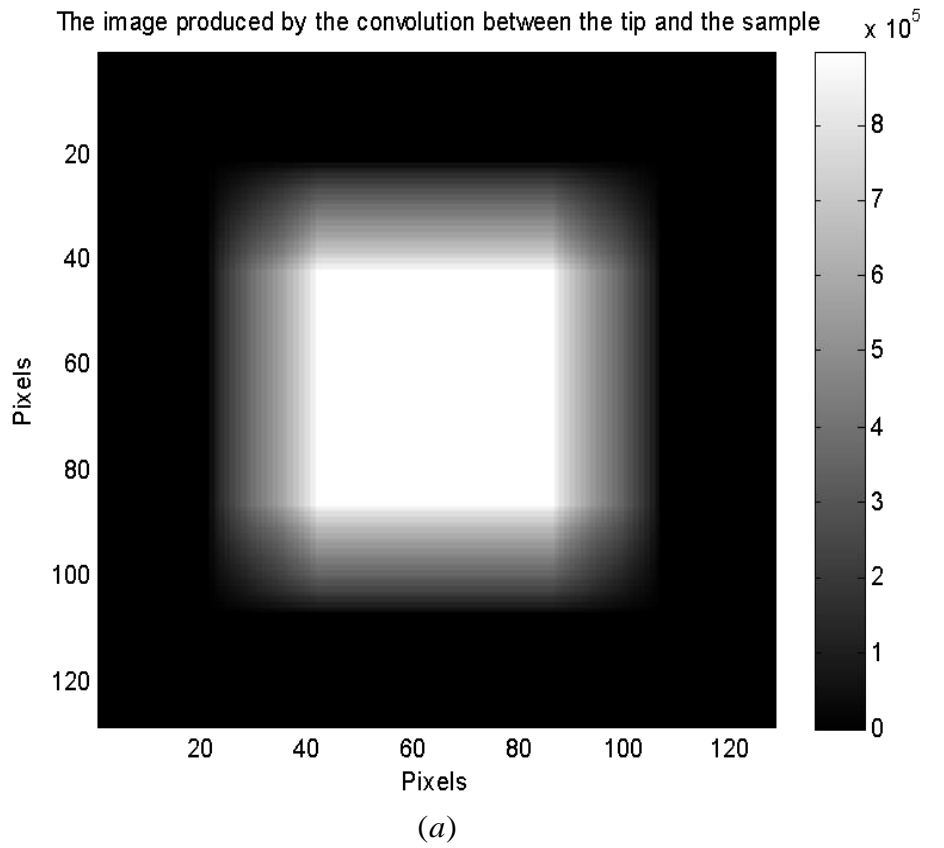


Fig. 4. Illustrates simulation results for the impulse response technique. (a) The image of the sample due to the convolution between the square sample and the tip; (b) the image of the square sample after applying a Lucy-Richardson deconvolution.

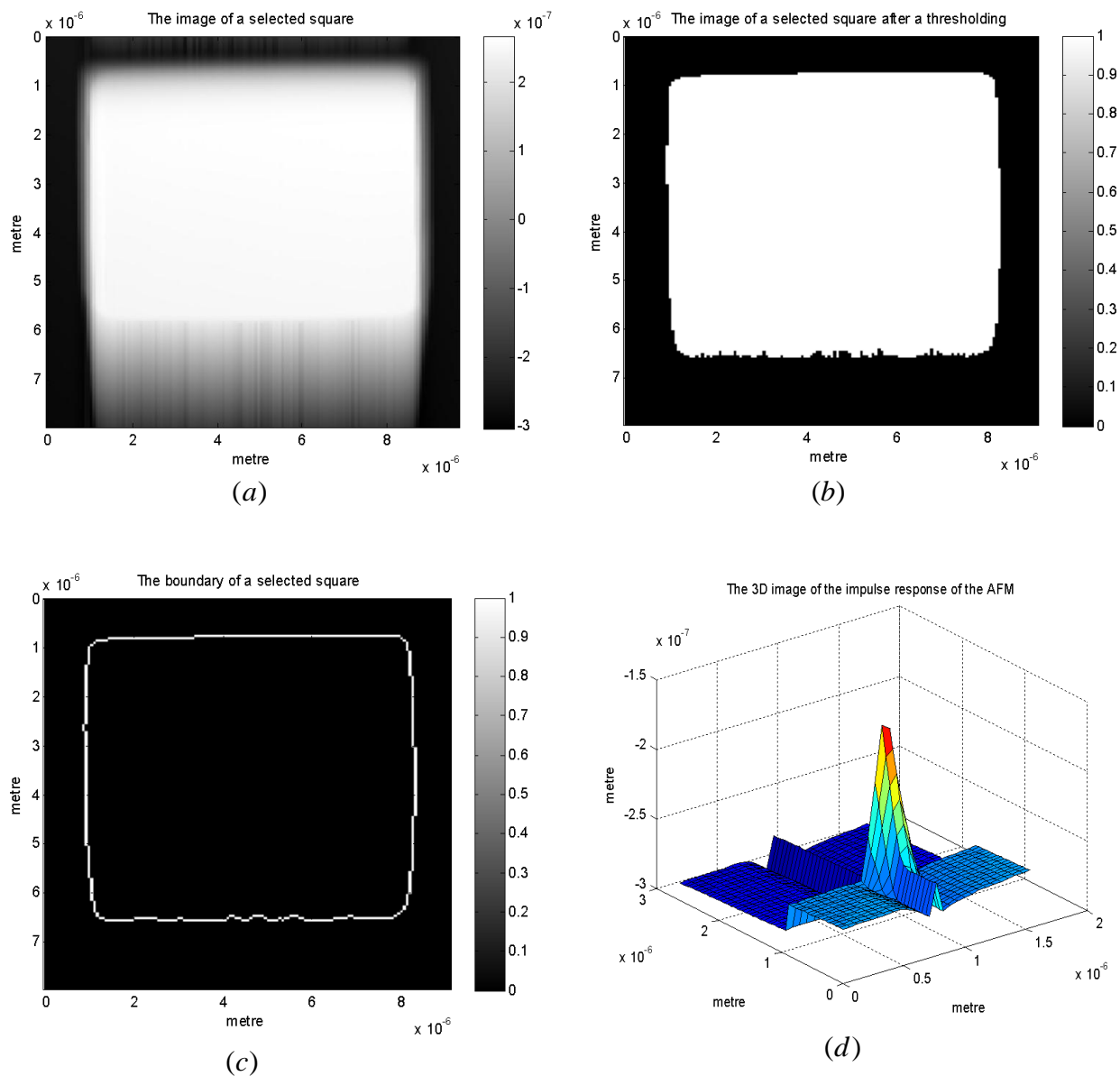


Fig. 5. Depicts the experimental results for the impulse response technique, produced using a real AFM characterizer sample that contains raised square pillars. (a) The square pillar sample; (b) Thresholding a standard sample that contains a single square pillar with known dimensions; (c) Determining the location of the square pillar in the image by defining the outer boundary for removing the pixels that belong to the square pillar from the image; (d) Extracting the tip shape of the AFM.

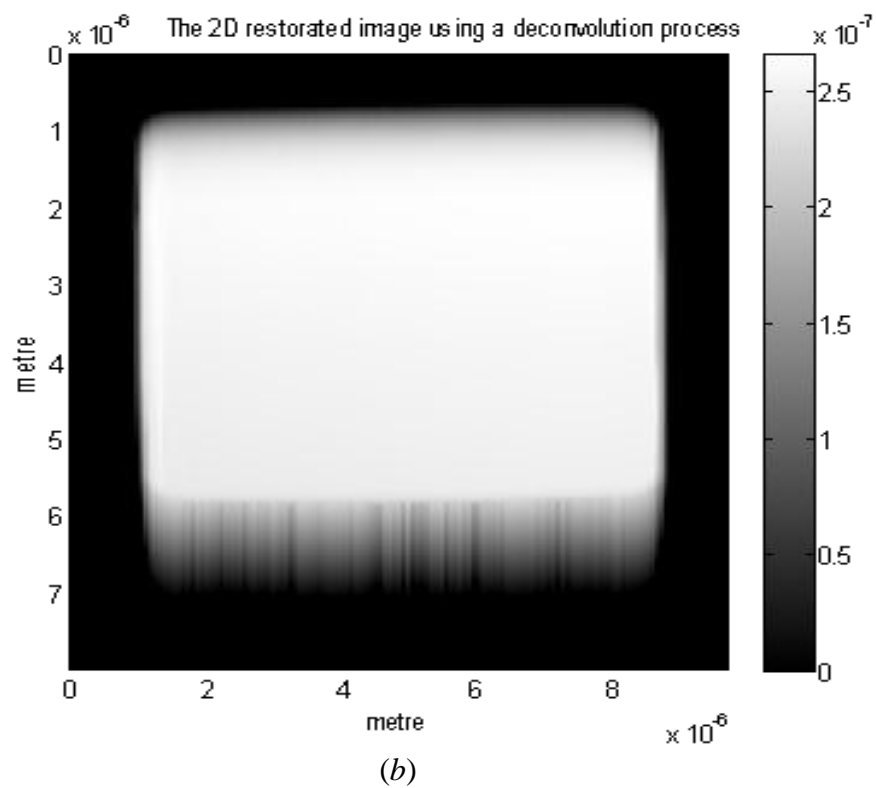
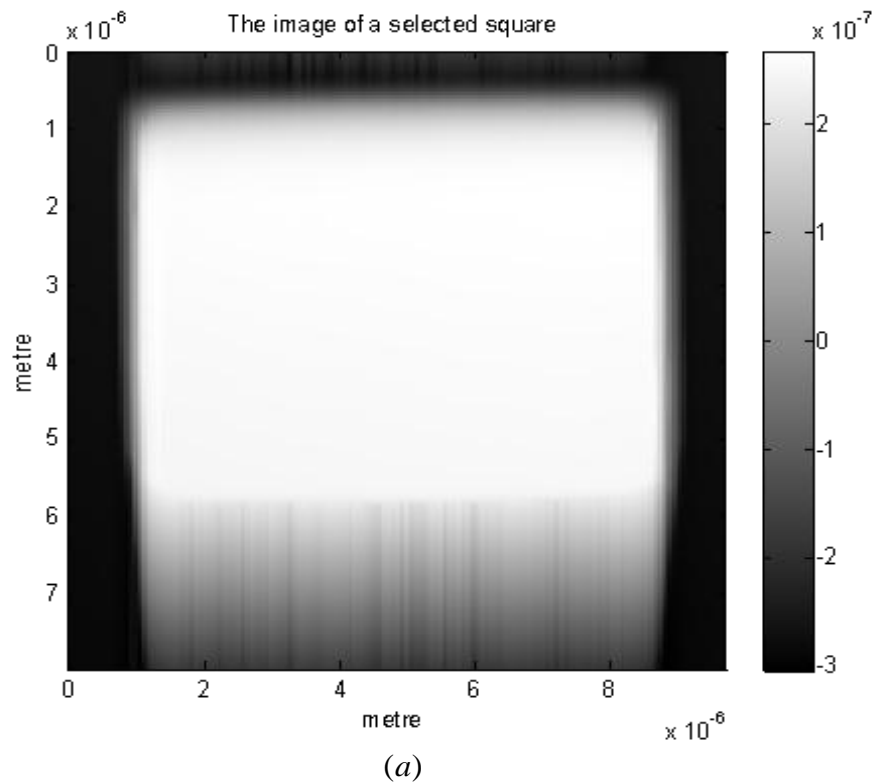


Fig. 6. Illustrates the experimental results for the impulse response technique using a Lucy-Richardson deconvolution algorithm for reconstructing a real AFM sample that contains raised square pillars. (a) The raw 2D AFM image of a real sample that contains a grid of raised square pillars measured using contact mode AFM; (b) The 2D image of the same sample after applying a Lucy-Richardson deconvolution algorithm (the restored image).

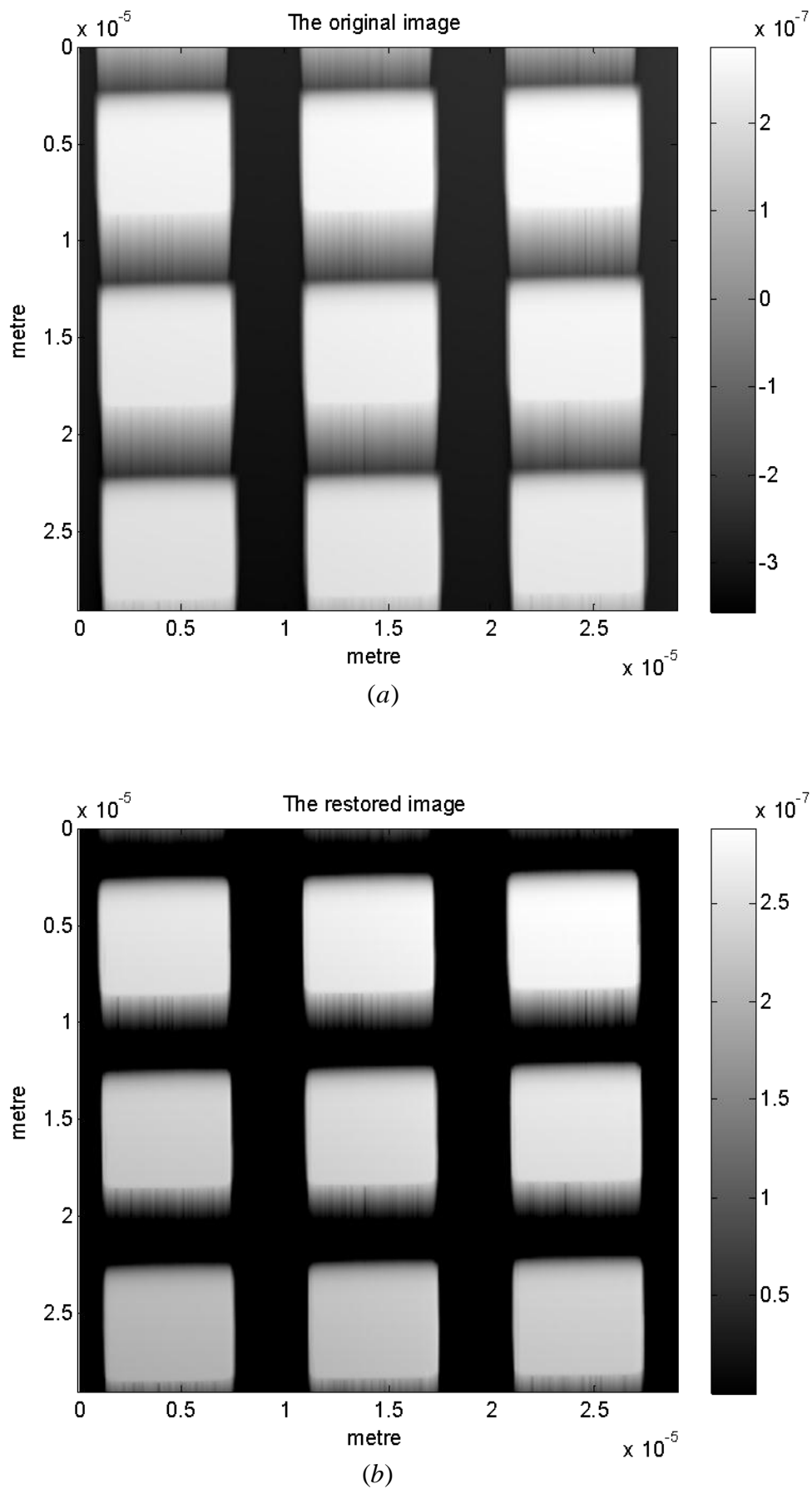


Fig. 7. Shows the experimental results for the impulse response technique using a Lucy-Richardson deconvolution method to restore the image of a real sample, consisting of a single raised square pillar. (a) The original image of the square pillar sample that was measured using the AFM; (b) the restored image of the square pillar sample after applying a Lucy-Richardson deconvolution algorithm.

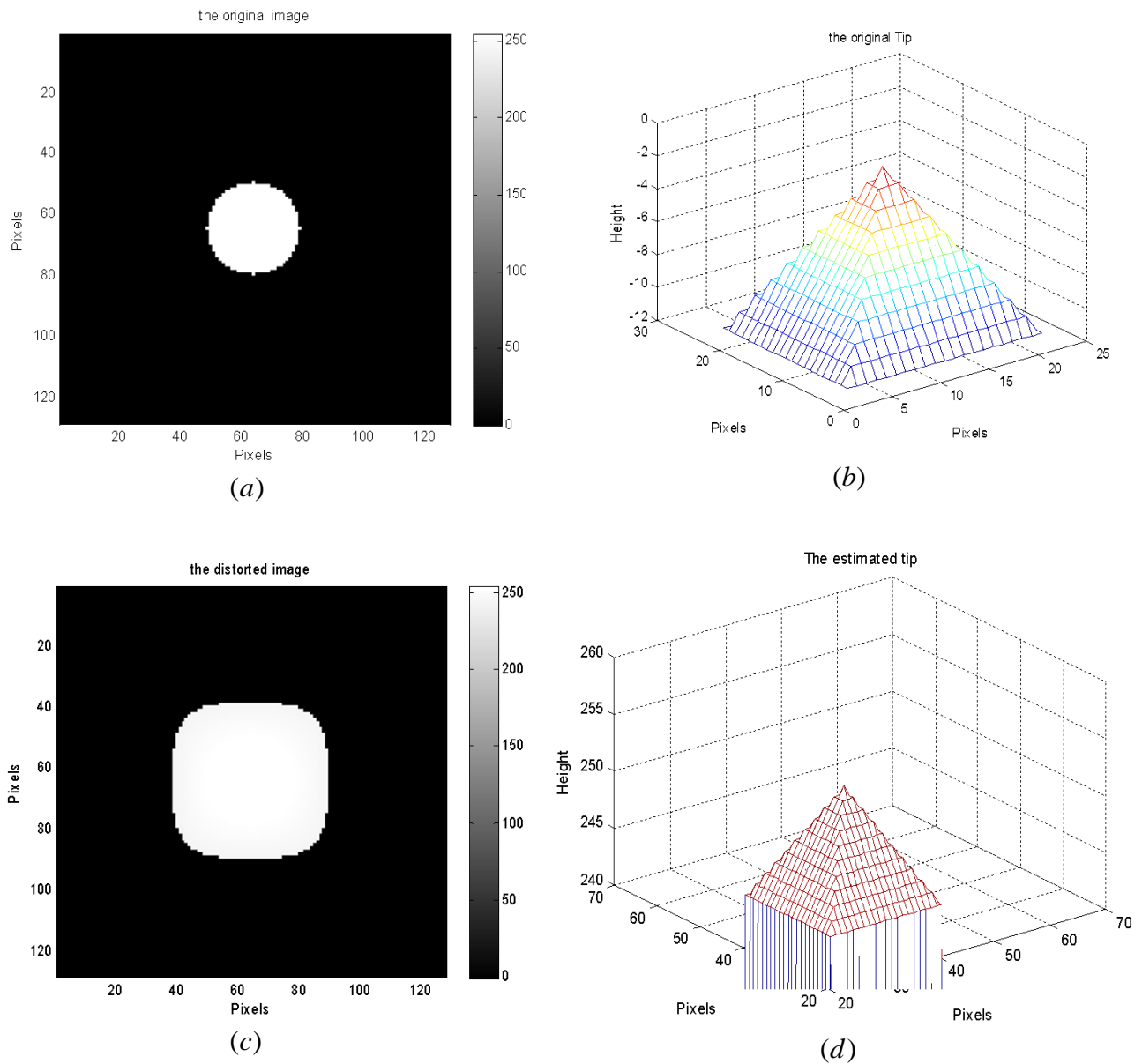
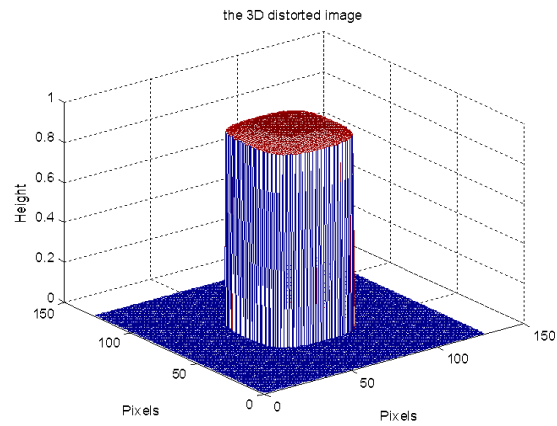
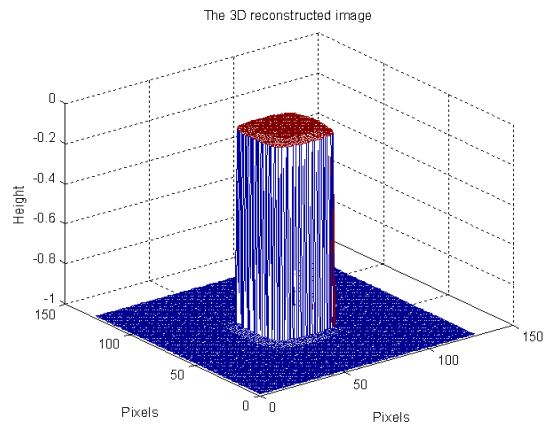


Fig. 9 Illustrates the results via computer simulation by using the impulse response technique:(a) The two-dimensional computer model of the sample; (b) The three-dimensional computer model of the AFM tip; (c) The two-dimensional simulated image of sample (d) The estimated tip shape produced by analyzing image (c).



(a)



(b)

Fig. 10 depicts a comparison between the degraded image and restored image achieved via computer simulation: (a) the degraded(dilated) image of the cylinder as it would be measured by a pyramidal AFM tip; (b) The restored image produced after applying an erosion operation between the dilated image and the reconstructed AFM tip.

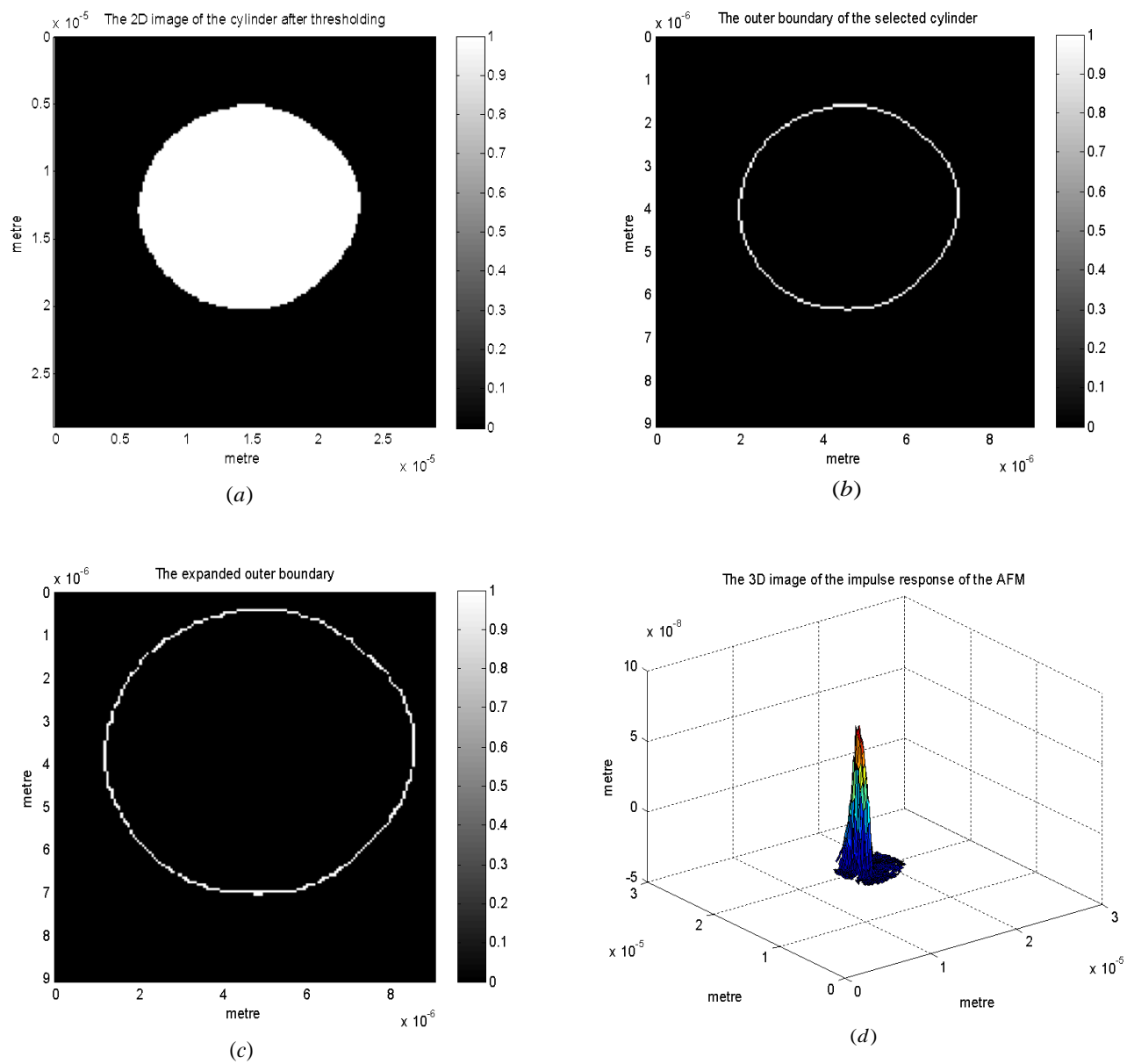


Fig. 11 Illustrates the steps of the experimental procedure for estimating the AFM tip: (a) thresholding a standard sample that contains a cylinder with known dimensions, (b) determining the location of the cylinder in the image by defining the outer boundary; (c) determining the outer boundary and the expanding outer boundary for removing the pixels that belong to the cylinder from the image; (d) extracting the tip shape of the AFM.

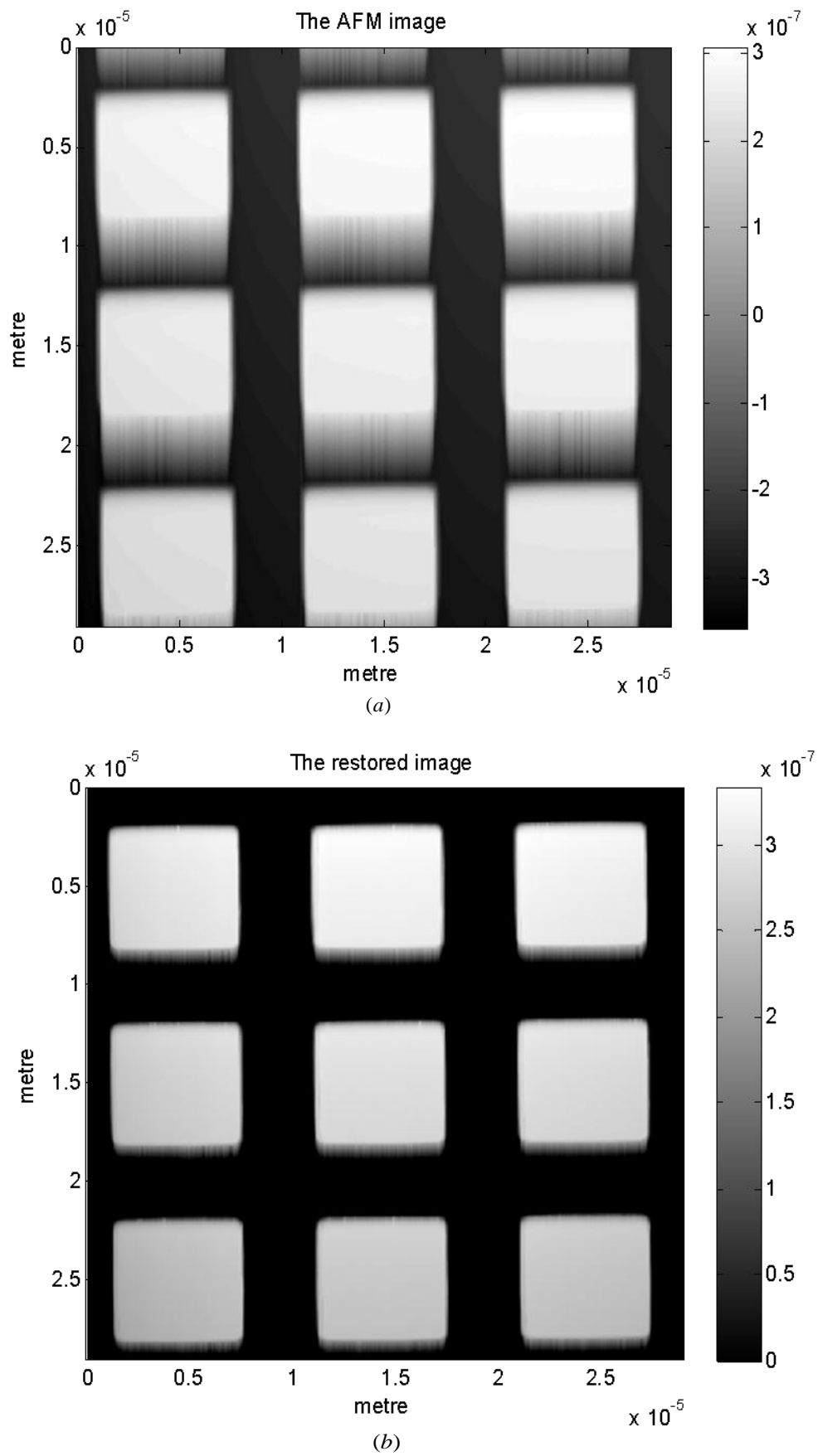
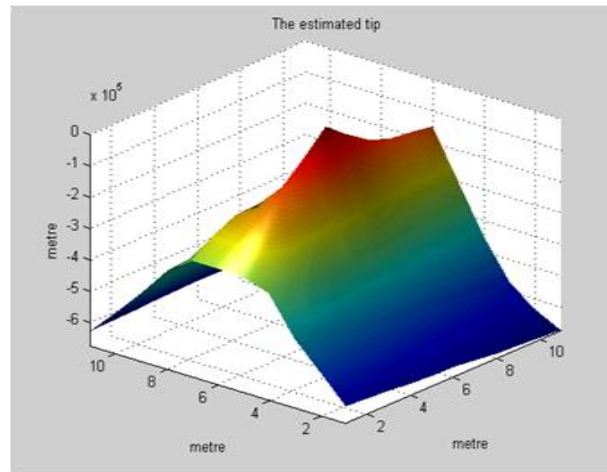
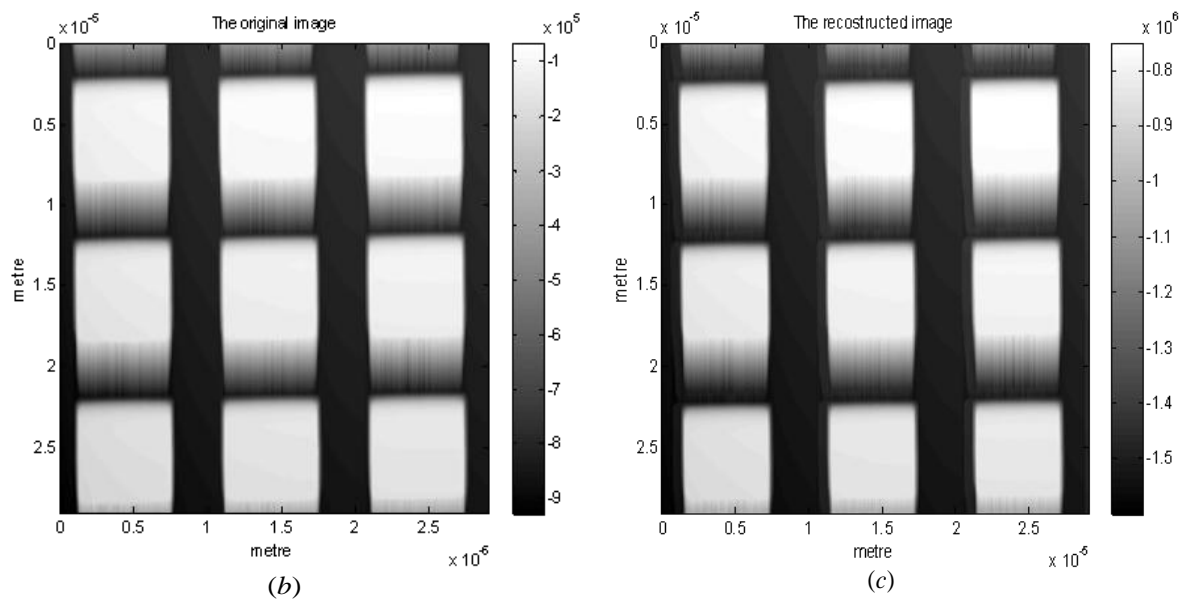


Fig. 12 depicts a comparison between the raw experimental AFM image and the restored AFM image that was produced using the proposed technique: (a) The image of the real sample that contains squares measured by a AFM tip; (b) The restored AFM image after applying a Lucy-Richardson deconvolution process between the AFM image and the estimated AFM tip.



(a)



(b)

(c)

Fig. 13 Shows the experimental results for blind tip reconstruction using a real sample that contains a grid of square pillars. (a) The 3D image of the reconstructed tip using a blind tip estimation algorithm; (b) the distorted 2D raw original AFM image of a real sample that contains square pillars; (c) the restored AFM image after applying the blind tip estimation algorithm.